# Impurities on graphene: Midgap states and migration barriers

T. O. Wehling,[1,*] M. I. Katsnelson,[2] and A. I. Lichtenstein[1]
[1]*I. Institut für Theoretische Physik, Universität Hamburg, Jungiusstraße 9, D-20355 Hamburg, Germany*
[2]*Institute for Molecules and Materials, Radboud University of Nijmegen, Heijendaalseweg 135, 6525 AJ Nijmegen, The Netherlands*
(Received 30 June 2009; published 26 August 2009)

Monovalent impurities on graphene can be divided into ionically and covalently bond impurities. The covalent impurities with one chemically active electron cause universal midgap states as the carbon atom next to the impurity is effectively decoupled from the graphene $\pi$ bands. The electronic structure of graphene suppresses migration of these impurities and makes the universal midgap very stable. This effect is strongest for neutral covalently bond impurities. The ionically bond impurities have migration barriers of typically less than 0.1 eV, which is about an order of magnitude less than their typical binding energies. An asymmetry between anions and cations regarding their adsorption sites and topology of their potential-energy landscape is predicted. In addition, the migration barrier for oxygen adatoms on graphene and their electronic structure is discussed. The barrier is found to be similar to that of monovalent covalently bond impurities.

DOI: 10.1103/PhysRevB.80.085428 PACS number(s): 73.20.Hb, 72.80.Rj, 73.61.Wp

## I. INTRODUCTION

The discovery of graphene[1] and its remarkable electronic properties[2–4] initiated great research interest in this material. Particularly prospective for applications is the extraordinarily high charge-carrier mobility $\mu$ in graphene.[1,5,6] In combination with a very-high Fermi velocity $v \approx 10^6$ m/s this makes micron mean-free paths routinely achievable.

Away from the neutrality point, the conductivity of graphene is weakly temperature dependent and approximately proportional to the carrier concentration $n$.[7,8] The mechanism causing this behavior and limiting the electron mobility in graphene is still under debate. Charged impurities are probably the simplest and thus the most natural candidate[9–11] for the dominant source of electron scattering in graphene. However, room-temperature experiments with gaseous adsorbates such as $NO_2$ have showed only a weak dependence of $\mu$ on charged impurity concentration.[12] Furthermore, recent experiments[13] did not find any significant dependence of $\mu$ on immersing graphene devices in high-$\kappa$ media such as ethanol and water (dielectric constants $\kappa \approx 25$ and 80, respectively) but this disagrees with another report[14] in which a few monolayers of ice increased $\mu$ in graphene by $\approx 30\%$. Because of the experimental controversy, alternative mechanisms such as scattering on frozen ripples[15] and resonant impurities[16,17] were discussed.

However, both these mechanisms also have some weak points, rather theoretical than experimental. There is still no real theory which would explain why the ripple structure becomes quenched and thus almost temperature independent. As for the resonant scatterers, in general, the closeness of the impurity quasilocal states to the neutrality point necessary to make this mechanism efficient looks just accidental. To discuss this as the main scattering mechanism one needs, at least, to clarify the mechanism which makes the resonant scatterers typical for graphene. Thus, the physics of charge-carrier mobility in graphene, crucially important for most of potential applications, is not clarified yet. Also, while impurities appear as undesirable residua from the graphene-production process, chemical functionalization of graphene relies on impurities for controlling its electronic properties as demonstrated recently for hydrogenated graphene (graphane).[18]

For judging which impurities might determine electron scattering in graphene and for optimizing chemical functionalization, the mechanisms determining the impurity mobility, i.e., their migration barriers and binding energies, need to be known: first, the migration barriers decide at which temperatures impurities will start moving along the graphene sheet resulting in possible cluster formation. Indeed, it has been shown that clusters of (charged) impurities lead to weaker electron scattering than the same amount of randomly distributed impurities.[19] Moreover, the migration barriers and adsorption energies allow to judge at which temperature impurities can be removed from the graphene sheets, e.g., by annealing. In this article, we first consider monovalent adsorbates and show that these can be divided into two separate groups regarding the bonding mechanism: ionically and covalently bond impurities. To this end, we present *ab initio* calculations on H, Li, Na, K, Cs, F, Cl, Br, I, $CH_3$, and OH adsorbates on graphene. For these systems the electronic structure (Sec. III) and migration barriers (Sec. IV) are analyzed. The covalently bond impurities cause a characteristic midgap state derived from the graphene electrons. This state turns out to be very stable, as graphene's conjugated $\pi$ bonds enhance the migration barriers of neutral covalently bond impurities. In Sec. V, the experimentally important case of oxygen adatoms is considered. Their migration barrier turns out to be 0.74 eV, which is highly above room-temperature thermal energies and well inside the range of barriers for covalent impurities discussed in the preceding sections.

## II. METHODS

For a first-principles description of the graphene adsorbate systems we performed density-functional calculations within the generalized gradient approximation[20,21] on $4 \times 4$ graphene supercells containing one impurity. The Vienna *ab initio* simulation package (VASP) (Ref. 22) with the projector augmented wave[23,24] basis sets has been used for solving the

 

resulting Kohn-Sham equations. In this way we obtained relaxed structures for the graphene adsorbate systems, total energies, and orbitally resolved local density of electronic states (LDOS). In the total-energy calculations and during the structural relaxations the $k$ meshes for sampling of the supercell Brillouin zone were chosen be as dense as a $24 \times 24$ and $12 \times 12$ $k$ mesh, respectively, when folded up to the simple graphene unit cell.

To find migration barriers for ionically bond impurities it is sufficient to perform structural relaxations with the impurities in three different high-symmetry adsorption sites: on top of a C atom ($t$ site), in the middle of a hexagon ($h$ site) and above the middle of a nearest-neighbor C-C bond ($b$ site). The covalent impurities cause strong distortion of the nearby bonds and require the minimum-energy paths to be calculated using the nudged elastic-band method.[25] As starting guess a linear interpolation between two adjacent stable configurations with three or more intermediate points has been chosen. To check for convergence of the migration barriers with the supercell size, we performed also calculations with $3 \times 3$ as well as $5 \times 5$ supercells for H adatoms and reproduced the barrier from the $4 \times 4$ supercell within an accuracy of 4%. Moreover, the convergence of the local density of states close to the impurity with the supercell size has been assured in this way.

## III. ELECTRONIC STRUCTURE OF MONOVALENT IMPURITIES ON GRAPHENE

The local electronic structure of graphene in the vicinity of adsorbates (Fig. 1) can be grouped into two classes. The LDOS in the vicinity of adsorbates, such as Li or Cl exhibits a sharp resonance close to Fermi level which is almost entirely localized at the impurity. Besides this peak, the LDOS at the nearest neighbor and at the next-nearest neighbor of the impurity exhibits the pseudogap characteristic for graphene. This is qualitatively different for the second group of impurities [Figs. 1(c) and 1(d)]. H and F adatoms cause a midgap state characteristic for Dirac fermions: with the bonding partner of the impurity in sublattice A the impurity state is localized in sublattice B and at the impurity atom.

Every stable atomic configuration under investigation can be strictly grouped either into the class of strongly or weakly hybridized impurities, as can be seen from Figs. 1(e) and 1(f): ionically bond impurities give rise to a sharp acceptor (donor) level below (above) the Dirac point at $E_D=0$. The LDOS of covalently bond impurities is much broader and exhibits characteristic resonances far below the Fermi level (between $-10$ and $-4$ eV) as well as a midgap state at the Fermi level.

As regards electron scattering this midgap state is mainly independent of the particular type of covalent impurity. The supercell band structures for H, $CH_3$, OH, and F covalently bond to graphene are shown in Fig. 2. The band structure of graphene with adsorbed H and $CH_3$ as well as those for graphene with F and OH adsorbates coincide close to the Fermi level despite the different internal structure of the adsorbates. The coupling of the midgap state and the graphene bands can be quantified in an *effective* impurity model $H$

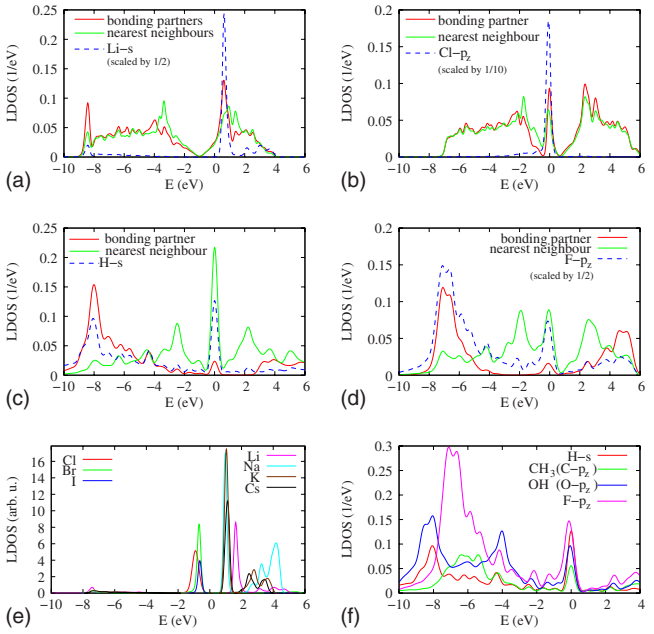


FIG. 1. (Color online) LDOS in different graphene-adsorbate systems. [(a)–(b)] ionically bond impurities and [(c)–(d)] covalently bond impurities. (a) Graphene + Li, (b) Graphene + Cl, (c) Graphene + H, and (d) Graphene + F. For the impurity's bonding partner in graphene and its nearest neighbor the $p_z$ projected LDOS is shown. The valence electron LDOS at the impurity site for ionically bond impurities is depicted in (e) and for covalently bond impurities in (f). In (a)–(d) and (f) the Fermi level is at $E=0$; in (e) the Dirac point is at $E=0$.

$=H_D+H_{\mathrm{imp}}$, where the unperturbed graphene bands are described by

$$H_D = \sum_k \epsilon(k) d_k^\dagger d_k \tag{1}$$

and the perturbation by

$$H_{\mathrm{imp}} = \epsilon_{\mathrm{imp}} c^\dagger c + V\left(\sum_k c^\dagger d_k + \mathrm{H.c.}\right). \tag{2}$$

Here, the index $k=(\vec{k},\nu)$ denotes crystal momentum $\vec{k}$ and band number $\nu=\pm$. $\epsilon(k)$ is the unperturbed graphene dispersion. The effective impurity is characterized by its energy $\epsilon_{\mathrm{imp}}$ and its hybridization $V$ with the graphene bands. In a

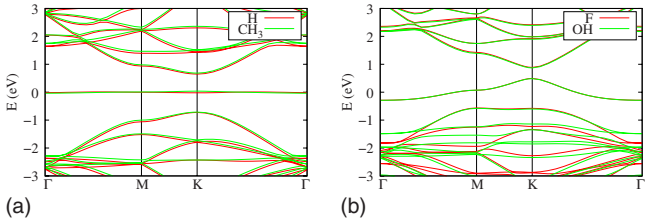


FIG. 2. (Color online) Supercell band structure of (a) H and $CH_3$ on graphene as well as (b) F and OH bond covalently to graphene. Bands coincide close to the Fermi level ($E=0$) despite the different internal structure of the impurities.

TABLE I. Impurity energy and hybridization for the effective impurity model of the midgap state for different impurities. All impurities are placed on top of a C atom, which is at the total-energy minimum for the covalently bond impurities and the anions Cl/Br but not for the cations Li and Na.

| | $\epsilon_{\mathrm{imp}}$ (eV) | $\lvert V\rvert$ (eV) | | $\epsilon_{\mathrm{imp}}$ (eV) | $\lvert V\rvert$ (eV) |
|---|---|---|---|---|---|
| H | −0.03 | 0.69 | Li | 1.17 | 0.11 |
| $CH_3$ | −0.11 | 0.70 | Na | 0.93 | 0.07 |
| OH | −0.70 | 0.65 | Cl | −0.79 | 0.21 |
| F | −0.67 | 0.65 | Br | −0.73 | 0.09 |

supercell calculation at the backfolded Dirac points $\vec{k}=K^{\pm}$, this model simplifies to

$$H=\begin{pmatrix} \epsilon_{\mathrm{imp}} & A & B \\ A^* & 0 & 0 \\ B^* & 0 & 0 \end{pmatrix}, \tag{3}$$

where the zero block stems from the graphene bands at the Dirac point and $A$ $(B)$ are the components of $V_k$ in the two different sublattices A (B). This allows to derive the coupling strengths $|V|=\sqrt{|A|^2+|B|^2}$ and $\epsilon_{\mathrm{imp}}$ from the density functional theory energies of the three bands closest to the Fermi level in the supercell calculation: We identify the energies of these bands at the supercell Brillouin zone $K$ point, $E_1 \leq E_2 \leq E_3$, with the eigenvalues of $H$ from Eq. (3): $\epsilon_0=0$ and $\epsilon_{\pm}=\epsilon_{\mathrm{imp}}/2 \pm \sqrt{|\epsilon_{\mathrm{imp}}/2|^2+|V|^2}$. By letting $\epsilon_0=E_2$ (i.e., choosing the energy offset such that $E_2=0$), $\epsilon_-=E_1$ and $\epsilon_+=E_3$, and solving for $\epsilon_{\mathrm{imp}}$ and $|V|^2$, we obtain the impurity energies and coupling strengths as shown in Table I.

The coupling $|V|$ is mainly independent of the internal structure of the covalently bond impurities. Hence, this midgap state appears as a universal feature of all monovalent impurities which are strongly bond to one of graphene's carbon atoms.

Bonding of H atoms to graphene and related electron scattering has been analyzed in.[26–28] For the bonding partner of H, the $\pi$ bond to its nearest carbon neighbors is broken and a $\sigma$ bond with the H adatom is formed. The carbon-bonding partner of H atoms has been found to be decoupled from the graphene $\pi$-electron system and the resulting local imbalance between the number of atoms belong to each of the two sublattices causes a midgap state. The band structures from Fig. 2 and the coupling constants from Table I show that same mechanism is effective for all monovalent covalently bond impurities on graphene.

It might appear surprising that F forms a covalent bond with graphene, while Cl becomes charged and bonds ionically. This is caused by the inertness of graphene's $sp^2$ network, which has to be broken upon formation of a covalent bond. For Cl having one completely filled inner electronic shell the typical covalent radius is 1.02 Å (see Ref. 29), which is almost twice more than for F. Thus, a significantly lower covalent binding energy can be expected for Cl than for F, which—as our calculations show—unables Cl to break graphene's $sp^2$ network. For the same reason, $NO_2$ does not bind covalently to graphene.

## IV. MIGRATION BARRIERS AND CHEMICAL BONDING

In the following we show, that the creation of the midgap state by an impurity covalently bond to one carbon atom enhances migration barriers for covalently bond monovalent impurities in graphene. A comparison to ionically bond impurities is given.

In agreement with Ref. 30, we find the energy minimum for the alkali cations at the $h$ sites and barriers as shown in Table II. The barriers decrease with cation size and are all (except for the special case of Li) below 0.1 eV. The potential-energy landscape for the cations consists of dips in the center of the hexagons bordered by a hexagonal net of banks. Within this net spanned by the nearest-neighbor carbon bonds, the variation of potential energy is by a factor of more than five smaller than between the $h$ site and the $t/b$ sites.

This landscape is reversed for the anions: having their energy minima on the net and maxima in the center of the hexagons, the anions can freely move on the graphene

TABLE II. Minimum-energy sites, bonding energies $E_b$, and migration barriers $\Delta E$ for ionically and covalently bond impurities.

| | Site | $E_b$ (eV) | $\Delta E$ (eV) | | Site | $E_b$ (eV) | $\Delta E$ (eV) | | Site | $E_b$ (eV) | $\Delta E$ (eV) |
|---|---|---|---|---|---|---|---|---|---|---|---|
| H | $t$ | 0.80 | 1.01 | Li | $h$ | 1.08 | 0.31 | Cl | $t,b$ | 0.80 | $<0.005$ |
| $CH_3$ | $t$ | 0.27 | 0.63 | Na | $h$ | 0.48 | 0.09 | Br | $t,b$ | 0.54 | $<0.005$ |
| OH | $t$ | 0.91 | 0.53 | K | $h$ | 0.81 | 0.06 | I | $t,b$ | 0.31 | $<0.005$ |
| F | $t$ | 1.99 | 0.29 | Cs | $h$ | 0.96 | 0.04 | | | | |
| O | $b$ | 2.43 | 0.74 | | | | | | | | |

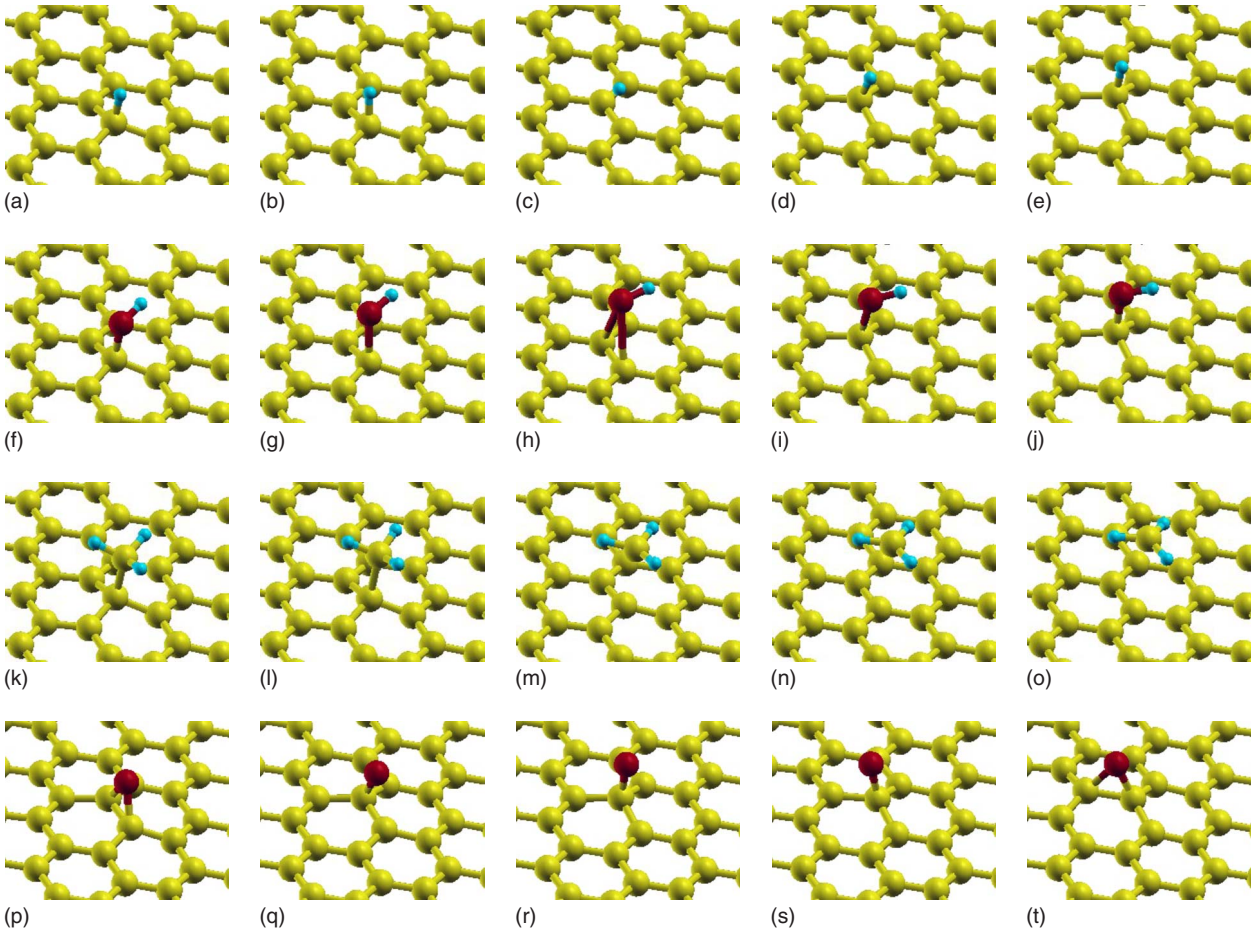


FIG. 3. (Color online) Stable- and transition-state geometries for H, OH, $CH_3$ and O (from top to bottom) on graphene. For H, OH, and O, two neighboring stable adsorption geometries are in the very right and left and the saddle-point transition state in the middle. Transition of $CH_3$ from one stable adsorbed geometry to a neighboring requires desorption. For $CH_3$, desorption with the saddle-point configuration being in the middle is shown. In the minimum-energy-adsorbed configuration of $CH_3$ the H-C-H bond angles are 109.2°, suggesting $sp^3$ hybridization of C in the $CH_3$ group, whereas the desorbed $CH_3$ is flat corresponding to $sp^2$ hybridization.

sheets. The fact that the height of the impurity above the sheet is always minimized in center of the hexagon, would result in the energy minimum being in the center of the hexagon for all ionically bond impurities if atomic-scale inhomogeneities in the screening charge of the impurities were negligible. The anions preferring the *t* and *b* sites over the *h* sites shows that inhomogeneities in the screening charge corrugate the potential-energy landscape of the ions on the order of some 10 meV.

The total bonding energy, $E_b$ (see Table II), is for the cationic species about 3 to an order of magnitude bigger than the migration barriers, $\Delta E$ associated with them. For the anions this ratio $E_b/\Delta E \sim 10^2$ is even larger. While the typical ionic bonding energies on the order of a few 100 meV to 1 eV prevent desorption a room temperature, the migration barriers are significantly smaller, make most ions mobile on graphene and let cluster formation appear possible at room temperature.

This is in strong contrast to covalently bond impurities: our calculations show that the potential-energy landscape for these impurities is by an order of magnitude more corrugated. We find migration barriers between 0.29 eV for F and 1.01 eV for H. Notably, F has highest absolute binding energy ($E_b$=1.99 eV) of all monovalent impurities considered, here, but it has the smallest migration barrier within the group of covalent impurities. For F and OH we find the saddle-point energy of the transition path significantly below the desorption energy, which is $E_b$=0.91 eV for OH. This is in strong contrast to H and $CH_3$: for H the energy of the saddle-point state is only 4 meV below the desorption barrier and moving a $CH_3$ group from one carbon atom to its nearest neighbor requires even overcoming the desorption barrier of 0.63 eV. No saddle-point configuration with the $CH_3$ group in the middle of two neighboring C atoms except for the $CH_3$ being fully desorbed from the graphene sheet could be found.

The transition paths between adjacent stable adsorption sites of H, OH, and $CH_3$ are depicted in Fig. 3. In agreement with previous studies,[26] we find significant out-of-plane lifting (0.4–0.5 Å) of the impurity's bonding partner in the minimum-energy configurations.

H, F, and OH are above a bridge site in saddle point of the transition path. In this configuration, the OH group is oriented perpendicular to the C-C bond of the two neighboring carbon atoms. For F, OH, and H the nature of chemical binding in the saddle-point configuration can be understood from

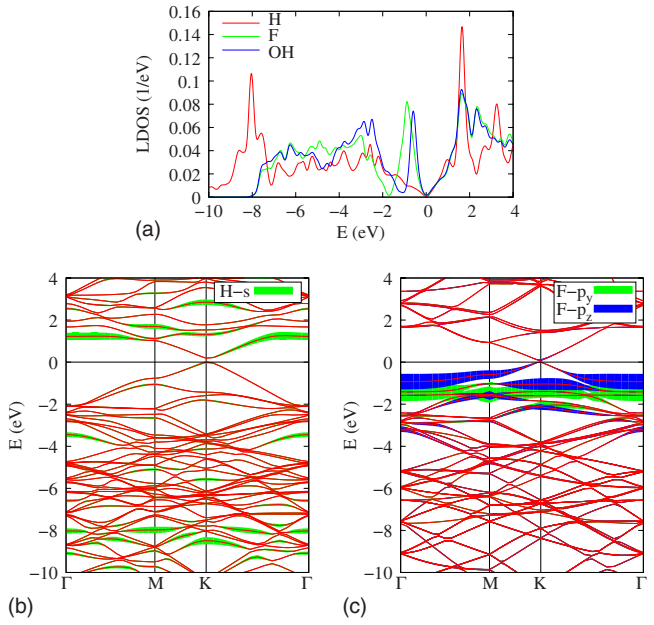


FIG. 4. (Color online) Electronic structure in the transition state. (a) $p_z$ LDOS at a carbon atom next to the impurity. Lower part: band structures of graphene supercells with (b) H and (c) F impurities in transition-state configuration. Contributions from the impurity atoms are marked as fatbands.

the supercell electronic properties shown in Fig. 4. The LDOS at the carbon atoms next to the F and OH impurities is very similar to the LDOS in the vicinity of *ionically* bond impurities, such as Cl or Br [see Fig. 1(b)]. This is in contrast to the case of H, where in addition to a resonance at 2 eV, the LDOS at the carbon neighbor of the impurity is broadened and exhibits a peak at −8 eV—similar to all covalently bond impurities in their minimum-energy configuration. The H impurity causes a donor level and is at the same time covalently bond as the supercell band structure with contributions from the H impurity marked as fat bands further illustrates. There are contributions from the H *s* orbital over the energy range from −10 up to +3 eV, indicating strong hybridization of the impurity orbital with the graphene bands. This is very different from F in the saddle-point configuration with its valence orbitals contributing significantly within an energy interval which is an order of magnitude smaller. In the transition state F and OH are ionically bond to graphene.

The high barrier for H suggests that the formation of a strong covalent bond in the transition state is highly unfavorable. The origin of this effect can be understood from the model Hamiltonian, Eq. (3): with the impurity on top of the bridge site, sublattice symmetry is preserved: $A=B$ in Eq. (3). The symmetric combination of the two C-$p_z$ orbitals adjacent to the impurity $\phi_+=\frac{1}{\sqrt{2}}(0,1,1)$ will couple to the impurity $\phi_{\text{imp}}=(1,0,0)$. The antisymmetric combination $\phi_-=\frac{1}{\sqrt{2}}(0,1,-1)$ is decoupled and forms the analog of the midgap state occurring for the impurity on top of a carbon atom: in the latter case, with the impurity's bonding partner in sublattice A, one obtains $B=0$ and finite $A$ in Eq. (3). Thus, $\phi_0=(0,0,1)$ is decoupled from the impurity in the stable configuration. $\phi_0$ is nonbonding and is therefore at the energy of the Dirac point. $\phi_-=\frac{1}{\sqrt{2}}(0,1,-1)$, however, is an antibonding combination of neighboring C-$p_z$ orbitals. The *ab initio* calculations show that the resonances derived from this state are more than 1 eV above the Dirac point, unoccupied and not available for screening the additional positive charge brought by the H impurity. Thus, the creation of a local charge is enforced by graphene's electronic structure for the impurity in a *b*-site saddle-point configuration. As a consequence, a strong tendency to ionic bonding with graphene *decreases* migration barriers while migration of preferably neutral covalently bond impurities is suppressed.

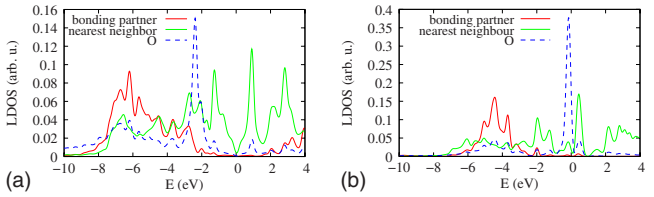


FIG. 5. (Color online) Electronic structure of graphene with adsorbed oxygen in the minimum-energy configuration (a) and in the transition state configuration (b). The $p_z$-projected LDOS at a carbon-bonding partner of oxygen, one of its nearest neighbors, and the LDOS at the oxygen adatom are shown.

## V. OXYGEN IMPURITIES ON GRAPHENE

In the previous sections, we showed with the model system of monovalent impurities that covalently bond impurities exhibit higher migration barriers than ionically bond impurities. With increasing number of chemically active orbitals, as, e.g., for transition-metal adsorbates with partially filled 3*d* shells, the situation can become arbitrarily complicated. We now show, however, that the experimentally and technically important case of oxygen adatoms is well in line with the results on monovalent impurities.

Oxygen being divalent, adsorbs to bridge sites on graphene with migration from one stable configuration to the next involving the path depicted in Fig. 3. In the stable adsorbed configuration, it binds covalently to graphene with decoupling its two carbon-bonding partners from the graphene $\pi$ electronic system (see Fig. 5). The LDOS at these carbon atoms is strongly depleted in the vicinity of the Fermi level and exhibits the typical shape of $sp^3$ bonded carbon—very similar to the situation for monovalent covalently bond impurities on graphene discussed in Sec. III. However, no midgap state is created by oxygen adatoms in their minimum-energy configuration as both graphene sublattices are affected equally by the oxygen adatoms. There are resonances in the LDOS of nearest neighbors at $E=-1.2$ eV and $E=0.9$ eV but the LDOS vanishes linearly at the Fermi level $E_F=0$. This is because O represents a "double impurity" in terms of a tight-binding model,[31,32] where strong impurities do not universally create midgap states.

For migration of oxygen from one stable configuration to a neighboring, one of its two bonds to graphene has to be broken. In the saddle-point state, oxygen is forming a single covalent bond to one carbon atom. This results in a midgap state of the same nature as in the case of covalently bonding

monovalent impurities in their stable configuration. The midgap state is slightly above the Fermi level as the nonbonding orbital of oxygen [sharp peak below $E_F=0$ in Fig. 5(b)] is fully below $E_F=0$ and accepts one electron from the midgap state. So, O binds partially covalent and partially ionically to graphene in the saddle-point configuration.

As in the case of monovalent impurities, the requirement of breaking one covalent bond results in the rather high migration barrier of 0.74 eV for oxygen on graphene, which is however smaller than the adsorption energy of 2.43 eV. In this sense O is similar to OH or F on graphene, which are all able to form a (partially) ionic bond in the saddle-point configuration.

## VI. CONCLUSIONS

In this paper we investigated various examples of monovalent impurities on graphene and established a relation between their type of chemical bonding, the occurrence of chiral midgap states and their migration barriers. We showed that migration barriers of ionically bond impurities are significantly lower than their binding energies, $\Delta E \ll E_b$, which is in contrast to covalently bond impurities having typical migration barriers on the order of some 100 meV to 1 eV and $\Delta E \sim E_b$.

This tendency explains experimental findings of charged impurities moving almost freely on graphene[12,33] and experiments suggesting considerable migration barriers for H adsorbates.[18,34] The fact that clusterization of impurities on graphene strongly suppresses their contribution to the resistivity[19] makes covalently bond impurities one natural candidate to the main source of scattering limiting the electron mobility in graphene. It is essential that, as demonstrated here, these impurities frequently have quasilocal peaks nearby the neutrality point—not accidentally but enforced by symmetry.

## ACKNOWLEDGMENTS

The authors thank A. Geim for inspiring discussions. Support from SFB 668 (Germany), FOM (The Netherlands) as well as computer time from HLRN are acknowledged.

*twehling@physnet.uni-hamburg.de

[1] K. S. Novoselov, A. K. Geim, S. V. Morozov, D. Jiang, Y. Zhang, S. V. Dubonos, I. V. Grigorieva, and A. A. Firsov, Science **306**, 666 (2004).
[2] A. K. Geim and K. S. Novoselov, Nature Mater. **6**, 183 (2007).
[3] M. I. Katsnelson, Mater. Today **10**, 20 (2007).
[4] A. H. Castro Neto, F. Guinea, N. M. R. Peres, K. S. Novoselov, and A. K. Geim, Rev. Mod. Phys. **81**, 109 (2009).
[5] K. I. Bolotin, K. J. Sikes, Z. Jiang, M. Klima, G. Fudenberg, J. Hone, P. Kim, and H. L. Stormer, Solid State Commun. **146**, 351 (2008).
[6] X. Du, I. Skachko, A. Barker, and E. Y. Andrei, Nat. Nanotechnol. **3**, 491 (2008).
[7] K. S. Novoselov, A. K. Geim, S. V. Morozov, D. Jiang, M. I. Katsnelson, I. V. Grigorieva, S. V. Dubonos, and A. A. Firsov, Nature (London) **438**, 197 (2005).
[8] Y. Zhang, Y.-W. Tan, H. L. Stormer, and P. Kim, Nature (London) **438**, 201 (2005).
[9] K. Nomura and A. H. Mac Donald, Phys. Rev. Lett. **96**, 256602 (2006).
[10] T. Ando, J. Phys. Soc. Jpn. **75**, 074716 (2006).
[11] S. Adam, E. H. Hwang, V. Galitski, and S. Das Sarma, Proc. Natl. Acad. Sci. U.S.A. **104**, 18392 (2007).
[12] F. Schedin, A. K. Geim, S. V. Morozov, E. W. Hill, P. Blake, M. I. Katsnelson, and K. S. Novoselov, Nature Mater. **6**, 652 (2007).
[13] L. A. Ponomarenko, R. Yang, T. M. Mohiuddin, M. I. Katsnelson, K. S. Novoselov, S. V. Morozov, A. A. Zhukov, F. Schedin, E. W. Hill, and A. K. Geim, Phys. Rev. Lett. **102**, 206603 (2009).
[14] C. Jang, S. Adam, J.-H. Chen, E. D. Williams, S. Das Sarma, and M. S. Fuhrer, Phys. Rev. Lett. **101**, 146805 (2008).
[15] M. I. Katsnelson and A. K. Geim, Phil. Trans. R. Soc. London, Ser. A **366**, 195 (2008).
[16] M. I. Katsnelson and K. S. Novoselov, Solid State Commun. **143**, 3 (2007).
[17] T. Stauber, N. M. R. Peres, and F. Guinea, Phys. Rev. B **76**, 205423 (2007).
[18] D. C. Elias, R. R. Nair, T. M. G. Mohiuddin, S. V. Morozov, P. Blake, M. P. Halsall, A. C. Ferrari, D. W. Boukhvalov, M. I. Katsnelson, A. K. Geim, and K. S. Novoselov, Science **323**, 610 (2009).
[19] M. I. Katsnelson, F. Guinea, and A. K. Geim, Phys. Rev. B **79**, 195426 (2009).
[20] J. P. Perdew, J. A. Chevary, S. H. Vosko, K. A. Jackson, M. R. Pederson, D. J. Singh, and C. Fiolhais, Phys. Rev. B **46**, 6671 (1992).
[21] J. P. Perdew, K. Burke, and M. Ernzerhof, Phys. Rev. Lett. **77**, 3865 (1996).
[22] G. Kresse and J. Hafner, J. Phys. Condens. Matter **6**, 8245 (1994).
[23] P. E. Blöchl, Phys. Rev. B **50**, 17953 (1994).
[24] G. Kresse and D. Joubert, Phys. Rev. B **59**, 1758 (1999).
[25] H. Jónsson, G. Mills, and K. W. Jacobsen, in *Classical and Quantum Dynamics in Condensed Phase Simulations*, edited by B. J. Berne, G. Ciccotti, and D. F. Coker (World Scientific, Singapore, 1998), p. 385.
[26] D. W. Boukhvalov, M. I. Katsnelson, and A. I. Lichtenstein, Phys. Rev. B **77**, 035427 (2008).
[27] S. Casolo, O. M. L. vvik, R. Martinazzo, and G. F. Tantardini, J. Chem. Phys. **130**, 054704 (2009).
[28] J. P. Robinson, H. Schomerus, L. Oroszlány, and V. I. Fal'ko, Phys. Rev. Lett. **101**, 196803 (2008).
[29] B. Cordero, V. Gomez, A. E. Platero-Prats, M. Reves, J. Echeverria, E. Cremades, F. Barragan, and S. Alvarez, Dalton Trans. **2008**, 2832.
[30] K. T. Chan, J. B. Neaton, and M. L. Cohen, Phys. Rev. B **77**, 235430 (2008).

[31] T. O. Wehling, A. V. Balatsky, M. I. Katsnelson, A. I. Lichtenstein, K. Scharnberg, and R. Wiesendanger, Phys. Rev. B **75**, 125425 (2007).
[32] T. O. Wehling, M. I. Katsnelson, and A. I. Lichtenstein, Chem. Phys. Lett. **476**, 125 (2009).
[33] M. Caragiu and S. Finberg, J. Phys.: Condens. Matter **17**, R995 (2005).
[34] J. C. Meyer, C. O. Girit, M. F. Crommie, and A. Zettl, Nature (London) **454**, 319 (2008).